**Trapezohedral platinum nanocrystals with high-index facets for high-performance hydrazine electrooxidation**

**Sheng-Nan Hu[1], Na Tian[1,*], Meng-Ying Li[2], Chi Xiao[1], Yao-Yin Lou[1,*], Zhi-You Zhou[1], Shi-Gang Sun[1]**

[1]State Key Laboratory of Physical Chemistry of Solid Surfaces, Collaborative Innovation Center of Chemistry for Energy Materials, College of Chemistry and Chemical Engineering, Xiamen University, Xiamen 361005, Fujian, China.
[2]Hubei Collaborative Innovation Center for Advanced Organic Chemical Materials & Key Laboratory for the Synthesis and Application of Organic Functional Molecules, Hubei University, Wuhan 430062, Hubei, China.

[*]**Correspondence to:** Prof. Na Tian, State Key Laboratory of Physical Chemistry of Solid Surfaces, Collaborative Innovation Center of Chemistry for Energy Materials, College of Chemistry and Chemical Engineering, Xiamen University, 422 Siming South Road, Xiamen 361005, Fujian, China. E-mail: tnsd@xmu.edu.cn; Dr. Yao-Yin Lou, State Key Laboratory of Physical Chemistry of Solid Surfaces, Collaborative Innovation Center of Chemistry for Energy Materials, College of Chemistry and Chemical Engineering, Xiamen University, 422 Siming South Road, Xiamen 361005, Fujian, China. E-mail: louyaoyin13@mails.ucas.ac.cn

## CHARACTERIZATION

The electrochemical tests of HzOR were performed in a three-electrode cell. Graphite rod and saturated calomel electrode (SCE) were used as counter electrode and reference electrode, respectively. All of the measured potentials were converted to reversible hydrogen electrode (RHE) according to the Nernst equation ($E_{RHE} = E_{SCE} + 0.242 + 0.059$ pH). Prior to each electrochemical measurement, the electrolyte solution was deoxygenated by bubbling high-purity $N_2$ for 20 min. The electrochemical measurements of HzOR were conducted in 0.5 M $N_2H_4$ + 1 M KOH solutions and the scan rate is 10 mV $s^{-1}$. The electrochemical impedance spectroscopy (EIS) was recorded in a frequency range from 0.1 Hz to 1 MHz at 0.20 V.

All calculation was carried out by using the density functional theory in the QE

package with the generalized gradient approximation of Perdew-Burke-Ernzerhof (GGA-PBE) to treat the exchange-correlation potential. The projector-augmented-wave (PAW) method was used to consider the electronic-ion interactions. The 2x2x1 Monkhorst-Pack k-point mesh was used for describing the Brillouin zones of Pt(311), Pt(111) and Pt(100). The bottom half Au atoms were fixed and all other atoms including intermediates were free during geometry optimizations. The cut-off energy was 400 eV and the vacuum region was above ~15 Å. Using the computational hydrogen electrode (p = 1 atm, T = 298 K). The Gibbs free energy was calculated from $G = E - TS$, in which $E$ is the total energy, $S$ is the entropy. The reaction energy of AH* $\rightarrow$ A*+ $H^+ + e^-$ was calculated from $\Delta G = E(A^*) + E(H^+ + e^-) - E(AH^*) - T\Delta S$. At the standard electrode potential condition, the free energy in the gas phase could be replaced by that of $H^+ + e^-$. Vibrational frequencies were calculated on the basis of the harmonic oscillator approximation.

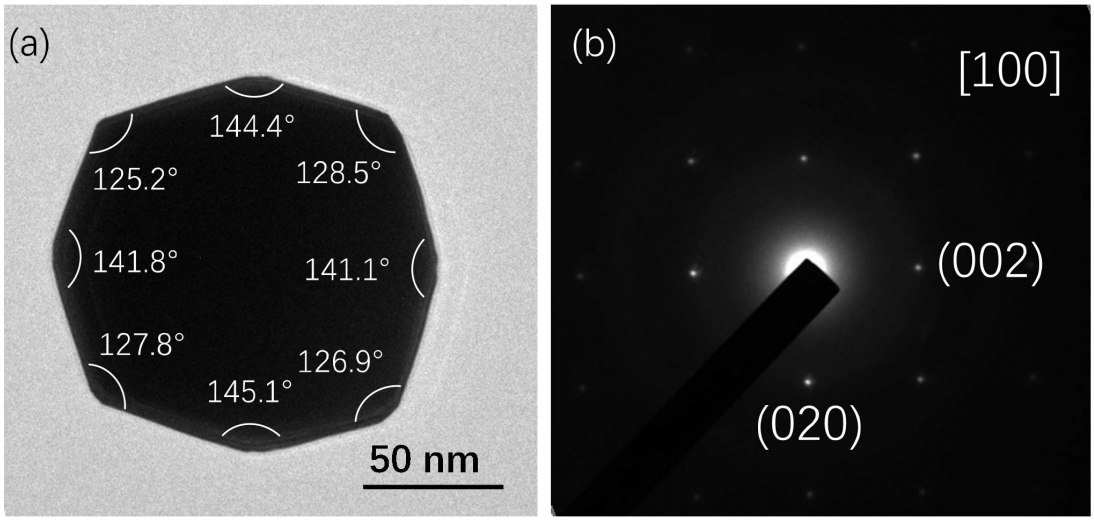


**Supplementary Figure 1.** TEM (a) and the corresponding SAED pattern (b) of the obtained TPH Pt-{311} nanocrystals along [001] direction. The surface facets were determined to be {311} by comparing the average value of the interfacial angles of $\bar{\alpha}$ with the theoretical ones. The average value of interfacial angle $\bar{\alpha}$ on the TPH Pt NCs is measured to be 143.1°, which is close to the theoretical value of α = 142.0° on a TPH NC enclosed by {311} facets.

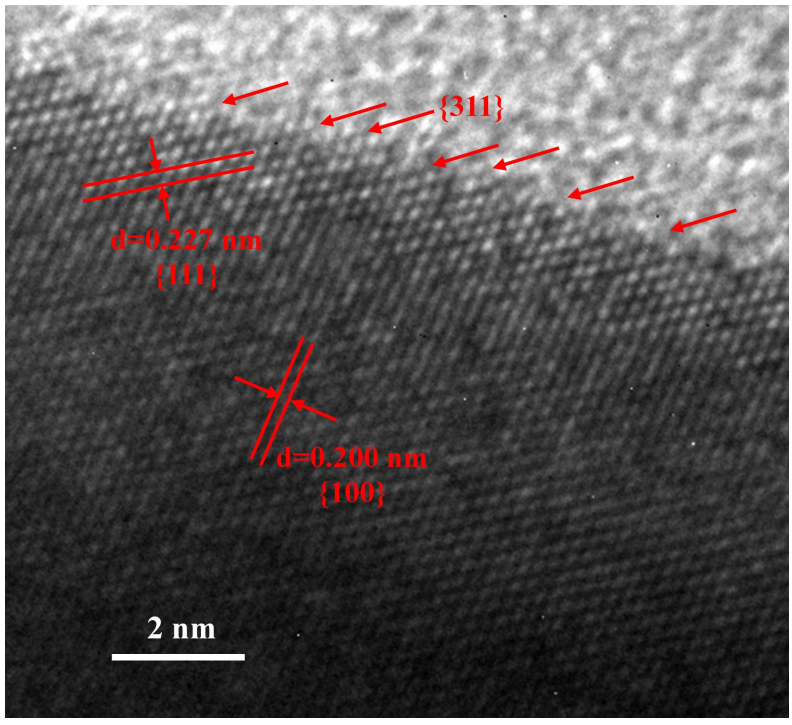


**Supplementary Figure 2.** HRTEM image of border atoms of a TPH Pt NC along <110> direction, showing the {311} surface sites.

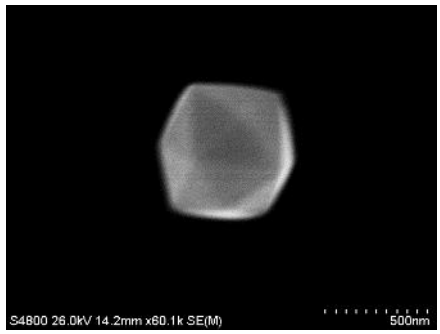


**Supplementary Figure 3.** SEM image recorded from TPH Pt NCs after 5000s test of HzOR.

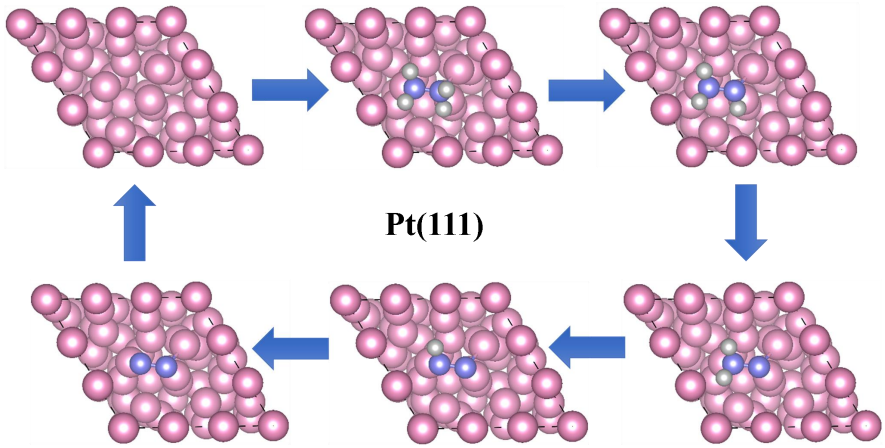


**Supplementary Figure 4.** Proposed pathway of the HzOR on Pt(111). The pink, blue and grey balls represent Pt, N and H atoms, respectively.

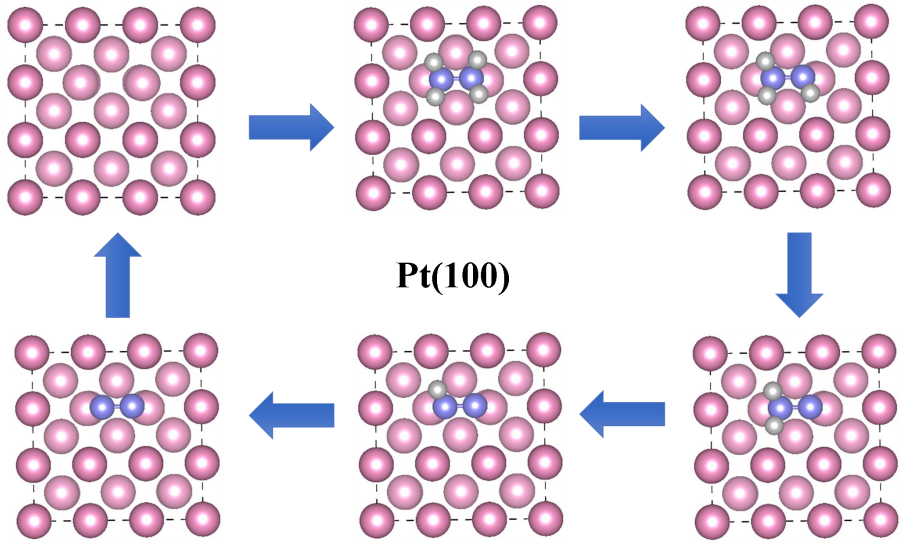


**Supplementary Figure 5.** Proposed pathway of the HzOR on Pt(100). The pink, blue and grey balls represent Pt, N and H atoms, respectively.

**Supplementary Table 1. Parameters of the programmed square-wave potential for preparation of Pt NCs**

| | Solution * | $E_N$ (V) | $t_N$ (ms) | $E_L$ (V) | $E_U$ (V) | $t_G$ (min) | $f$ (Hz) | Miller indices | Microfacet notation | $d_{step}$ ($\times 10^{14}$) | CNs |
|---|---|---|---|---|---|---|---|---|---|---|---|
| TPH Pt NCs | a | 0 | 140 | 0.42 | 1.39 | 30 | 100 | {311} | 2(111) × (100) | 7.83 | 7 |
| OTH Pt NCs | b | 0.05 | 140 | 0.38 | 1.30 | 8 | 100 | {111} | (111) | / | 9 |
| Cubic Pt NCs | a | 0 | 140 | 0.34 | 1.36 | 20 | 100 | - | - | - | - |
| | c | - | - | 0.45 | 1.50 | 15 | 100 | {100} | (100) | / | 8 |

*a: 2.0 mM $H_2PtCl_6$ + 0.1 M $H_2SO_4$; b: 2.0 mM $H_2PtCl_6$ + 0.1 M $Na_2SO_4$; c: 0.1 M $H_2SO_4$. $E_N$ is the nucleation potential; $t_N$ is the time stay at the nucleation potential; $E_L$ and $E_U$ are the lower and upper potential, respectively; $f$ is the frequency of square-wave potential; $t_G$ is the time of the square-wave potential for the growth of Pt NCs; CNs: Coordination numbers.

**Supplementary Table 2. Calculation of ECSA of the Pt NCs**

| | $Q_H$/μC | ECSA/cm$^2$ |
|---|---|---|
| TPH Pt-{311} NCs | 227 | 1.08 |
| OTH Pt-{111} NCs | 195 | 0.93 |
| Cubic Pt-{100} NCs | 200 | 0.95 |

**Supplementary Table 3. Estimation of Pt loading of all studied Pt NCs**

| | NO. | Area ($\times 10^{-8}$ cm$^2$) | D (nm) | Mass density ($\times 10^{-6}$ g cm$^{-2}$) | Formula of volume | Loading ($\times 10^{-6}$ g) |
|---|---|---|---|---|---|---|
| TPH Pt-{311} NCs | 185 | 28.53 | 139 | 19.55 | $\pi D^3/6$ | 5.5 |
| OTH Pt-{111} NCs | 249 | 18.11 | 110 | 9.35 | $D^3/4.2$ | 2.6 |
| Cubic Pt-{100} NCs | 124 | 9.48 | 91 | 21.14 | $D^3$ | 6.0 |

*D is the diameter of Pt nanocrystals.

**Supplementary Table 4. Comparison of HzOR activity of TPH Pt-{311} NCs with the reference results**

| Catalyst | Electrolyte | Potential (V *vs.* RHE) | Overpotential (V) | Current density ($mA \cdot cm^{-2}$) | Ref. |
|---|---|---|---|---|---|
| **TPH Pt-{311} NCs** | 1 M KOH + 0.5 M $N_2H_4$ | 0.2<br>0.3<br>0.4 | 0.53<br>0.63<br>0.73 | 41.7<br>94.2<br>143.8 | This work |
| **Pt wire** | 1 M KOH + 0.5 M $N_2H_4$ | 0.2 | 0.53 | 32 | 1 |
| **Co NPs** | 1 M KOH + 0.5 M $N_2H_4$ | 0.3 | 0.63 | 75 | 2 |
| **HPHMC900** | 3 M KOH + 1 M $N_2H_4$ | 0.6 | 0.93 | 40 | 3 |
| **TOH Au NCs** | 0.1 M NaOH + 10 mM $N_2H_4$ | 0.4 | 0.73 | 122 | 4 |
| **CoNi-R-S** | 0.1 M KOH + 20 mM $N_2H_4$ | 0.3 | 0.63 | 2.5 | 5 |
| **$NiSe_2$** | 1 M KOH + 0.3 M $N_2H_4$ | 0.2 | 0.53 | 25 | 6 |
| **Ni foam@Ag-Ni** | 1 M KOH + 25 mM $N_2H_4$ | 0.5 | 0.83 | 1.2 | 7 |
| **Rh NCs** | 1 M KOH + 1 M $N_2H_4$ | 0.5 | 0.83 | 25 | 8 |
| **$FeS_2$** | 1 M KOH + 0.1 M $N_2H_4$ | 0.6 | 0.93 | 15 | 9 |
| **PdNiRu NCNs** | 0.5 M KOH + 10 mM $N_2H_4$ | 0.5 | 0.83 | 28 | 10 |

**REFERENCES**


1. Li J, Zhang C, Zhang C, Ma H, Yang Y, Guo Z, Wang Y, Ma H. Electronic configuration of single ruthenium atom immobilized in urchin-like tungsten trioxide towards hydrazine oxidation-assisted hydrogen evolution under wide pH media. *Chem Eng J* 2022;430:132953.

2. Chen S, Wang C, Liu S, Huang M, Lu J, Xu P, Chen Q. Boosting hydrazine oxidation reaction on CoP/Co mott-schottky electrocatalyst through engineering active sites. *J PhysChem Lett* 2021;12:4849-56.

3. Dhiman N, Pradhan D, Mohanty P. Heteroatom (N and P) enriched nanoporous carbon as an efficient electrocatalyst for hydrazine oxidation reaction. *Fuel* 2022;314:122722.

4. Liu F, Jiang X, Wang H, Chen C, Yang Y, Sheng T, Wei Y, Zhao X, Wei L.

Boosting electrocatalytic hydrazine oxidation reaction on highindex faceted Au concave trioctahedral nanocrystals. *ACS Sustain Chem Eng* 2022;10:696-70.

5. Zhou L, Shao M, Zhang C, Zhao J, He S, Rao D, Duan X. Hierarchical CoNi-sulfide nanosheet arrays derived from layered double hydroxides toward efficient hydrazine electrooxidation. *Adv Mater* 2016;29:1604080.

6. Feng Z, Wang E, Huang S, Liu J. Bifunctional nanoporous Ni-Co-Se electrocatalyst with superaerophobic surface for the water and hydrazine oxidation. *Nanoscale* 2020;12:4426-34.

7. Lei Y, Liu Y, Fan B, Mao L, Yu D, Huang Y, Guo F. Facile fabrication of hierarchically porous Ni foam@Ag-Ni catalyst for efficient hydrazine oxidation in alkaline medium. *J Taiwan Inst Chem E* 2019;105: 75-84.

8. Huang X, Wang Y, Zhu Q, Zhou K, Zhi H, Yang J. High quality synthesis of Rh nanocubes and their application in hydrazine hydrate oxidation assisted water splitting. *Inorg Chem Commun* 2021;134:109023.

9. Sun J, Liu C, Kong W, Liu J, Ma L, Li S, Xu Y. Rational design of FeS2 microspheres as high-performance catalyst for electrooxidation of hydrazine. *J Mater Sci Technol* 2022;110:161-66.

10. Yuan T, Wang A, Fang K, Wang Z, Feng J. Hydrogen evolution-assisted one-pot aqueous synthesis of hierarchical trimetallic PdNiRu nanochains for hydrazine oxidation reaction. *J Energy Chem* 2017;26:1231-37.